Observation of guided and reflection P-waves in urban ambient noise cross-correlograms

Yunyue Elita Li, Enhedelihai Nilot, National University of Singapore, and Xuan Feng, Jilin University

SUMMARY

Passive seismic methods have attracted increasing attention in recent years in applied geophysics, thanks to its nonintrusive imaging and monitoring ability. Particularly, crosscorrelograms of ambient noise have been used as approximations to the Green's functions between pairs of receivers. It has been widely reported that the crosscorrelograms are consisted of overwhelmingly surface waves and weak refracted P-waves. We present P-guided and P-reflected waves observed from the ambient noise crosscorrelograms in the urban environment of Singapore. We verify these observations based on simulated urban noise originated from road traffic traveling perpendicular to the geophone array. We show that when source location is fixed with respect to the receiver array, all simulated wave modes, including surface wave, directly arriving P-wave, and reflection P-wave, are present in the crosscorrelograms. The crosscorrelograms approximate the Green's functions of the transmission modes between pairs of receivers. For reflections, velocity information remains in the curvature of the events, but depth information cancels out by crosscorrelation.

INTRODUCTION

Crosscorrelation is widely used in passive seismology to image the subsurface at global (e.g. Shapiro et al. (2005)), regional (e.g. Yao et al. (2006)), and local scales (e.g. Chang et al. (2016)). In these studies, large receiver arrays (km to hundreds of km) are often used, together with long time recordings (month- to year-long data). These data are then crosscorrelated and summed to enhance the signal-to-noise ratio of the resulting crosscorrelation function, which approximates the Green's function between a pair of receivers. It is shown that the approximated Green's function is dominated by strong surface waves, which are used for inversion, tomography, and monitoring.

Recently, passive seismic imaging has attracted increasing attention in urban environment for near surface imaging due to its nonintrusive nature (Zhang et al., 2019) and its wide potential of incorporating distributed acoustic sensing technology (Dou et al., 2017; Spica et al., 2019; Fang et al., 2020). In contrast to regional studies, these urban studies utilize smaller geophone or fiber sensing array (tens to hundreds of meters), and shorter recording times (hours to weeks). The efficiency in space and time is needed for urban applications as they are limited by the urban built environment and the timeliness of urban monitoring requirements. Moreover, urban near surface applications often require a much higher spatial resolution compared to regional applications, usually down to meter scale. Therefore, conventional processing of ambient noise based on surface wave inversion and tomography cannot fully satisfy their need.

Since first conjectured by Claerbout (1968), many researchers have provided theoretical and numerical examples that all wave modes, including both surface and body waves, exist in the cross-correlation functions, and can be used for ambient noise imaging (Snieder, 2004; Wapenaar, 2004). Later, refracted P-waves are observed from cross-correlations of ambient noise when a relative short array is used to record month-long data (Roux et al., 2005; Poli et al., 2012b; Nakata et al., 2015). Although theoretical and numerical studies suggest that reflected P-waves should exist in the crosscorrelation functions (Wapenaar et al., 2002; Snieder et al., 2006), the seek for reflected P-wave in ambient noise field recording has been less successful. Instead, researchers turn to autocorrelation functions of ambient noise where multiple reflected P-waves may be preserved for subsurface imaging (Poli et al., 2012a; Oren and Nowack, 2016; Zhang et al., 2019).

The main contribution of this abstract is to show that two additional types of P-waves (guided and reflected) can also be observed in the crosscorrelograms of urban ambient noise. The observations are further validated using theoretical stationary phase analysis and numerical simulations of the urban ambient noise field.

FIELD ACQUISITION AND DATA PROCESSING

In this section, we present two field cases where both surface propagating Rayleigh waves and P-waves are retrieved from the crosscorrelation of urban ambient noise. In both cases, a short ($\leq$ 200 m) linear array with 24 vertical geophones is deployed. Both site locations are within quiet parks in the northeast region of Singapore, minimizing noise source within the array.

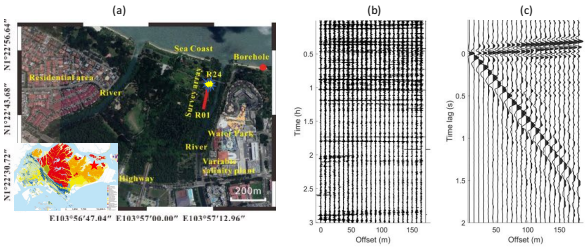

Figure 1: (a) Site map. (b) Recorded ambient noise. (c) Crosscorrelograms of the ambient noise.

Figure 1(a) shows the layout of the receivers at Site 1 and its location (denoted by the red star) in the insert. Site 1 is right on the northern coast of Singapore, with shallow artificial reclaimed material sitting on top of a sequence of Old Alluvium sedimentary formations and Bukit Timah granite bedrock. The geophone array is deployed linearly perpendicular to the coastline to the north and a highway 500 m to the south.

Figure 1(b) shows the 3-hour noise recorded every 2 ms at Site 1. The raw data appear to be uncorrelated in time for each receiver. However, strong coherent events can be clearly identified across the array.

Figure 1(c) shows the spatial-temporal correlation function with Receiver 24 as the master station. The crosscorrelograms are clearly asymmetric and reveal two different wave trains. In the positive time lags, a slow (around 200 m/s), low frequency, and dispersive wave train is observed. Considering the propagation direction from north to south, this wave is likely the Rayleigh wave induced by ocean waves. In the positive time lags, a fast (around 2000 m/s), high frequency, and dispersive wave train is observed. This wave is clearly originated from the south of the array, where all urban activities including traffic, construction, and manufacturing happen.

To further validate the observations, we take the positive and negative sides of the crosscorrelograms, and perform slant stack in the frequency domain to obtain the dispersion maps, shown in Figure 2(a) and (b), respectively. The black dash line on each plot denotes the picked dispersion curve for each wave. The maps shows strong dispersive signature for both the high frequency and the low frequency waves. Although it is common to observe the dispersion nature at the low frequencies for Rayleigh waves, it is the first time, to our best knowledge, a strong dispersion is observed from ambient noise at such high frequencies. The combination of high frequency and high velocity suggests that this is a P-guided wave, trapped in the shallow soft formation between the air and deep granite bedrock. We later verify this conjecture using simulated noise and its crosscorrelograms.

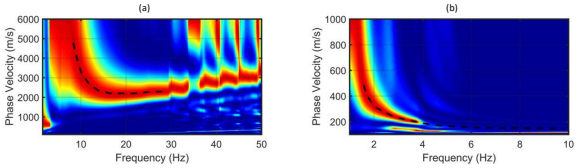

Figure 2: (a) Phase velocity map for the high-frequency, high speed wave in the negative lags of the crosscorrelograms. Notice the strong dispersive signature of the wave. (b) Phase velocity map for the low-frequency, low speed wave in the positive lags of the crosscorrelograms.

Figure 3 shows a similar experiment at Site 2, slightly more inland than Site 1. The geophone array is deployed east to west, perpendicular to the major noise source of the highway less than 100 m to the west. A total of 100 minutes worth of urban noise is processed, and the crosscorrelograms are shown in Figure 3(c). The correlation function is evidently dominated in the positive time lags, indicating the noise is predominately from west to east. Besides the commonly observed slow (500 m/s) Rayleigh wave, two hyperbolic events are also observed at much higher apparent velocities.

Similarly, dispersion maps are calculated to analyze the observation and shown in Figure 4. The dispersion map with the full frequency band shows three wave trains: a highly dispersive slow wave (around 500 m/s) train at low frequencies, an

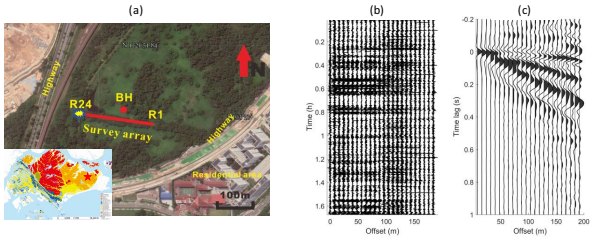

Figure 3: (a) Site map. (b) Recorded ambient noise. (c) Crosscorrelograms of the ambient noise.

intermediate-speed wave (around 1000 m/s) train at intermediate frequencies, and an fast wave (around 3500 m/s) train at high frequencies. Although the two high velocity waves are not entirely constant in their respective frequency bands, they are clearly not dispersive compared to the low frequency Rayleigh wave (Figure 4(b)). Given the apparent velocity and the curvature of the events, we suggest that these two events are P-reflections events, which we will verify in the subsequent section. To our best knowledge, this is the first time that P-reflection events are observed in the crosscorrelograms of the ambient noise.

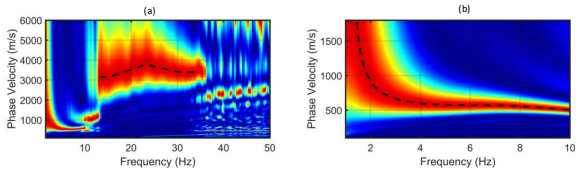

Figure 4: (a) Phase velocity map of the cross-correlograms. Notice the separation between the high frequency, high velocity wave and the low frequency, low velocity wave. (b) Zoom-in view of the phase velocity map at low frequencies. Notice the dispersive signature of the low frequency wave.

SIMULATING URBAN AMBIENT NOISE

In this section, we present the modeling principles for urban ambient noise field and the simulation results to match the field observations. We model the ambient noise field in an urban environment where 1) noise sources are distributed on the surface and outside of the array, and 2) the shallow subsurface is layered. Ambient data in the frequency domain can be represented as:

$$d(x,\omega) = \underbrace{\sum_{i=1}^{N_s} \frac{a_i}{|x-x_i^s|} e^{-i\omega\left(t_i+\frac{|x-x_i^s|}{v_s(\omega)}\right)}}_{①} + \underbrace{\sum_{i=1}^{N_s} \frac{a_i}{|x-x_i^s|} e^{-i\omega\left(t_i+\frac{|x-x_i^s|}{v_p(\omega)}\right)}}_{②} + \underbrace{\sum_{i=1}^{N_s}\sum_{j=1}^{N_r} a_i r_j e^{-i\omega\left(t_i+\frac{1}{v_j}\sqrt{(x-x_i^s)^2+4z_j^2}\right)}}_{③} + n(x,\omega), \quad (1)$$

where N_s and N_r are the number of sources and reflectors, respectively. The onset time t_i, location x_i^s, and amplitude a_i

for $i = 1, \cdots, N_s$ sources are random variables. v_j, z_j, and r_j for $j = 1, \cdots, N_r$ are the average velocity, the depth, and the reflectivity for the j^{th} layer, respectively. $v_p(\omega)$ and $v_s(\omega)$ are the phase velocity of the guided P-wave and the Rayleigh wave, respectively. We model other sources of noises using $n(x, \omega)$.

In Equation 1, term ① denotes the Rayleigh wave, term ② denotes the guided P-wave, and term ③ denotes the reflections. Without losing generality, we assume the sources are all on one side of the array, that is $x > x_i^s$ for all sources. The cross-correlation between recordings at a "master trace" $x = x_0$ with all traces consists of the following six terms:

$$\begin{aligned} d(x_0,\omega)\overline{d(x,\omega)} &= ①_0\overline{①}+①_0\overline{②}+①_0\overline{③} \\ &+ ②_0\overline{①}+②_0\overline{②}+②_0\overline{③} \\ &+ ③_0\overline{①}+③_0\overline{②}+③_0\overline{③}. \end{aligned} \quad (2)$$

In the following subsections we analyze each term for the most general case and a special case in an urban environment.

Random source locations, random source times

In the most general case, where source locations are randomly distributed around the array and sources are excited at random times, the first diagonal term reads:

$$\begin{aligned} ①_0\overline{①} &= \sum_{i=1}^{N_s} \frac{a_i^2}{(x_0-x_i^s)(x-x_i^s)} e^{-i\frac{\omega}{v_s(\omega)}(x_0-x)} \\ &+ \sum_{i\neq j}^{N_s} \frac{a_i a_j}{(x_0-x_i^s)(x-x_j^s)} e^{-i\frac{\omega}{v_s(\omega)}(v_s(\omega)(t_i-t_j)+(x_0-x)-(x_i^s-x_j^s))}. \end{aligned} \quad (3)$$

The first term in Equation 3 is the Green's function for the surface wave from x_0 to x, up to a scaling factor. It gets constructively stacked with more noise sources. The second term is the "crosstalk" noise between different sources. Since t_i and x_i^s are both random variables, adding more noise sources together will reduce the amplitude of the crosstalk due to destructive interference of sine waves with random phase shifts.

Similarly, the second diagonal term reads

$$\begin{aligned} ②_0\overline{②} &= \sum_{i=1}^{N_s} \frac{a_i^2}{(x_0-x_i^s)(x-x_i^s)} e^{-i\frac{\omega}{v_p(\omega)}(x_0-x)} \\ &+ \sum_{i\neq j}^{N_s} \frac{a_i a_j}{(x_0-x_i^s)(x-x_j^s)} e^{-i\frac{\omega}{v_p(\omega)}(v_p(\omega)(t_i-t_j)+(x_0-x)-(x_i^s-x_j^s))}, \end{aligned} \quad (4)$$

with the first term in Equation 4 the Green's function for the guided P-wave from x_0 to x, and the second term vanishing with more random sources.

The third diagonal term is more complicated with multiple chances for crosstalks from different sources, and different reflectors:

$$\begin{aligned} ③_0\overline{③} &= \sum_{i=1}^{N_s}\sum_{j=1}^{N_r} a_i^2 r_j^2 e^{-i\omega\left(\frac{1}{v_j}\left(\sqrt{(x_0-x_i^s)^2+4z_i^2}-\sqrt{(x-x_i^s)^2+4z_i^2}\right)\right)} \\ &+ \sum_{i\neq n}^{N_s}\sum_{j\neq m}^{N_r} a_i a_n r_j r_m e^{-i\omega\left(t_i-t_n+\frac{1}{v_j}\sqrt{(x_0-x_i^s)^2+4z_j^2}-\frac{1}{v_m}\sqrt{(x-x_n^s)^2+4z_m^2}\right)} \end{aligned} \quad (5)$$

where both terms tend to vanish when N_s is large and x_i^s are randomly distributed.

Similar analysis can be performed for all off-diagonal terms in Equation 2 to deduce that all off-diagonal terms approach zero when N_s is large and x_i^s are randomly distributed. Therefore, in the most general case, if the sources are truly randomly distributed in space and time, the only remaining terms in the cross-correlation function correspond to the approximated Green's function for the transmission waves. No body wave reflections can be preserved after stacking cross correlation functions over a long period of time.

Figure 5(a) shows the simulated ambient noise where random sources are placed at random locations along the line of the receiver array, with one side generating surface wave, the other generating both guided and reflection P-wave. Uncorrelated Gaussian noise is added to simulate other unmodeled noise. Although cannot be compared point-by-point with the recorded ambient noise in Figure 1(b), the overall statistical characteristics of the simulated noise agree well with the field recordings.

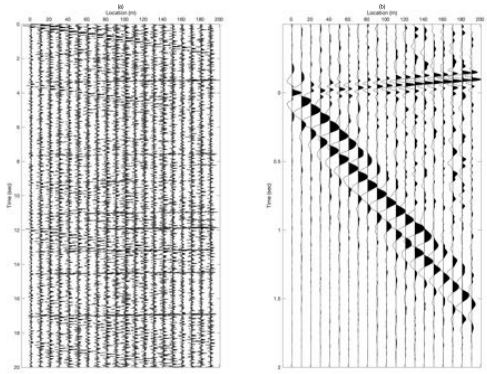

Figure 5: (a) Synthetic ambient noise. (b) Cross-correlograms of the synthetic ambient noise.

Figure 5(b) shows the cross-correlograms that also agree well with the field data result in Figure 1(c). It is evident that although the sources generate both guided and reflection P-waves (i.e. these wave modes exist in the ambient noise recordings), the crosscorrelation and summation process filters out the reflection events via destructive summation and enhances the transmitted P-guided wave via constructive summation.

Fixed source locations, random source times

Urban ambient noise sources are often more predictable in their location than their time. When a linear array is deployed perpendicular to a busy road, the source location is fixed in the 2D section illuminated by the linear array, that is $x_i^s = x_j^s = x^s$, for any i and j. On the contrary, the time for each car passing by is truly random. Under this special condition, the remaining terms after stacking over sources are:

$$①_0\overline{①} = \sum_{i=1}^{N_s} \frac{a_i^2}{(x_0-x^s)(x-x^s)} e^{-i\frac{\omega}{v_s(\omega)}(x_0-x)}. \quad (6)$$

$$②_0\overline{②} = \sum_{i=1}^{N_s} \frac{a_i^2}{(x_0-x^s)(x-x^s)} e^{-i\frac{\omega}{v_p(\omega)}(x_0-x)}. \quad (7)$$

$$③_0\overline{③} = \sum_{i=1}^{N_s}\sum_{j=1}^{N_r} a_i^2 r_j^{2k} e^{-i\omega\left(\frac{1}{v_j}\left(\sqrt{(x_0-x^s)^2+4z_i^2}-\sqrt{(x-x^s)^2+4z_i^2}\right)\right)} \quad (8)$$

The remaining term in $③_0\overline{③}$ represents shifted body wave reflections by the reflection arrival times at the master trace. This term preserves the curvature of the P-wave reflections, while loses the most of the depth information since only relative moveout in an event is kept.

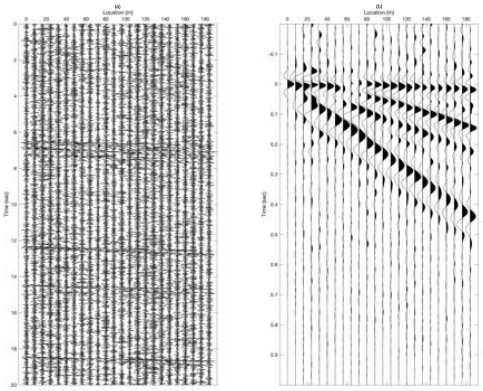

Figure 6: (a) Synthetic ambient noise. (b) Cross-correlograms of the synthetic ambient noise.

Figure 6(a) shows the simulated ambient noise where random sources are placed at a fixed location with respect to the receiver array, emitting Rayleigh waves, direct P waves, and reflection P-waves. Different realizations of uncorrelated random Gaussian noise are added to simulated other unmodeled noise sources. Again, the simulated noise clearly captures the statistical characteristics of the recorded ambient noise in Figure 3(b).

Figure 6(b) shows the cross-correlograms that contains not only the strong Rayleigh wave, but also two reflection events with hyperbolic curvatures. The similarity between the simulated and field recording cross-correlograms validates our observations that the high frequency, high velocity events are indeed P-wave reflections. In fact, extensive (although non-exhaustive) experiments show that none of the trials with random source locations could reproduce a similar cross-correlation function as in Figure 3(c).

DISCUSSIONS

Previous studies on ambient noise cross-correlations show that the correlograms are overwhelmed by the strong surface waves, Rayleigh waves for vertical recordings, and love waves for horizontal recordings. With smaller station spacing, refracted P-waves have also been observed. To the best of our knowledge, guided and reflection P-waves are observed for the first time in our study.

Urban activities such as traffic, construction, and manufacturing, as well as natural activities such as ocean waves and wind could generate all wave modes propagating in the medium, albeit with different partition in amplitudes. To excite guided P-wave, special geological conditions such as strong contrast between free surface and bedrock have to be satisfied. Additionally, high frequency noise sources above the guided-P cutoff frequency are also needed. These conditions are rarely satisfied, even in an urban environment. Among the 7 sites that we have collected urban ambient noise, P-guided waves are only observed on Site 1 (Figure 1). Via simulations, we experiment with various distributions of the random noise sources, and conclude that the dispersive signature of the observed event cannot be reproduced unless a P-guided wave is excited. Analysis of the observed P-guided wave defines the depth of the bedrock and the P-wave velocity, which helps to constrain the underdetermined surface wave dispersion inversion.

Refracted and reflected P-waves excited by ambient noise sources looses its amplitude faster compared to surface waves due to spherical spreading (compared to circular spreading) and Earth's larger attenuation for higher frequencies. Therefore, P-waves are more often observed in smaller geophone/seismometer arrays. For reflected P-waves, additional amplitude attenuation may happen when ambient noise records are cross-correlated and stacked to increase signal-to-noise ratio, especially in the cases where the noise sources are randomly distributed in space. Via simulation, we verify that if the source location is fixed, relative kinematics difference of reflected P-waves across the array can be preserved in the cross-correlograms, although the absolute traveltime information is lost. Due to the strong traffic noise source, we observed similar reflection P-wave events at 4 out of 7 sites. Joint interpretation of the surface and P-reflections in the cross-correlograms should better constrain the subsurface model building using urban ambient noise recordings.

CONCLUSIONS

We present two field cases where guided and reflected P-waves are observed in the cross-correlograms of urban ambient noise. To the best of our knowledge, it is the first time that these wave modes are reported in passive seismic data processing. To verify the observations, we simulate the urban noise field in a layered medium based on explicit formulations of Green's functions. Standard processing on the simulated noise field shows that even if the noise sources may trigger all wave modes in the ambient noise recordings, the cross-correlation and stacking process enhances the transmission modes via constructive summation and destroy the reflection modes via destructive summation in the most general case when noise sources are randomly distributed around the receiver array. Nonetheless, when noise source location is fixed, relative kinematic information of the P-wave reflections are preserved in the cross-correlograms.

ACKNOWLEDGEMENTS

The authors acknowledge the EDB Petroleum Engineering Professorship for financial support.

REFERENCES

Chang, J. P., S. A. de Ridder, and B. L. Biondi, 2016, High-frequency rayleigh-wave tomography using traffic noise from long beach, californiatomography using traffic noise: Geophysics, **81**, B43–B53.

Claerbout, J. F., 1968, Synthesis of a layered medium from its acoustic transmission response: Geophysics, **33**, 264–269.

Dou, S., N. Lindsey, A. M. Wagner, T. M. Daley, B. Freifeld, M. Robertson, J. Peterson, C. Ulrich, E. R. Martin, and J. B. Ajo-Franklin, 2017, Distributed acoustic sensing for seismic monitoring of the near surface: A traffic-noise interferometry case study: Scientific reports, **7**, 11620.

Fang, G., Y. E. Li, Y. Zhao, and E. R. Martin, 2020, Urban near-surface seismic monitoring using distributed acoustic sensing: Geophysical Research Letters, **47**.

Nakata, N., J. P. Chang, J. F. Lawrence, and P. Boué, 2015, Body wave extraction and tomography at long beach, california, with ambient-noise interferometry: Journal of Geophysical Research: Solid Earth, **120**, 1159–1173.

Oren, C., and R. L. Nowack, 2016, Seismic body-wave interferometry using noise auto-correlations for crustal structure: Geophysical Journal International, ggw394.

Poli, P., M. Campillo, H. Pedersen, L. W. Group, et al., 2012a, Body-wave imaging of earth?s mantle discontinuities from ambient seismic noise: Science, **338**, 1063–1065.

Poli, P., H. Pedersen, and M. Campillo, 2012b, Emergence of body waves from cross-correlation of short period seismic noise: Geophysical Journal International, **188**, 549–558.

Roux, P., K. G. Sabra, P. Gerstoft, W. Kuperman, and M. C. Fehler, 2005, P-waves from cross-correlation of seismic noise: Geophysical Research Letters, **32**.

Shapiro, N. M., M. Campillo, L. Stehly, and M. H. Ritzwoller, 2005, High-resolution surface-wave tomography from ambient seismic noise: Science, **307**, 1615–1618.

Snieder, R., 2004, Extracting the green?s function from the correlation of coda waves: A derivation based on stationary phase: Physical Review E, **69**, 046610.

Snieder, R., K. Wapenaar, and K. Larner, 2006, Spurious multiples in seismic interferometry of primaries: Geophysics, **71**, SI111–SI124.

Spica, Z., M. Perton, E. R. Martin, B. Biondi, and G. Beroza, 2019, Urban seismic site characterization by fiber-optic seismology: EarthArXiv.

Wapenaar, K., 2004, Retrieving the elastodynamic green's function of an arbitrary inhomogeneous medium by cross correlation: Physical review letters, **93**, 254301.

Wapenaar, K., D. Draganov, J. Thorbecke, and J. Fokkema, 2002, Theory of acoustic daylight imaging revisited, *in* SEG Technical Program Expanded Abstracts 2002: Society of Exploration Geophysicists, 2269–2272.

Yao, H., R. D. van Der Hilst, and M. V. De Hoop, 2006, Surface-wave array tomography in se tibet from ambient seismic noise and two-station analysis?i. phase velocity maps: Geophysical Journal International, **166**, 732–744.

Zhang, Y., Y. E. Li, H. Zhang, and T. Ku, 2019, Near-surface site investigation by seismic interferometry using urban traffic noise in singapore: Geophysics, **84**, B169–B180.